

Supporting Information: Imaging magnetic switching in orthogonally twisted stacks of a van der Waals antiferromagnet

Alexander J. Healey,¹ Cheng Tan,^{1,2} Boris Gross,³ Sam C. Scholten,⁴ Kaijian Xing,¹ Daniel G. Chica,⁵ Brett C. Johnson,¹ Martino Poggio,^{3,6} Michael E. Ziebel,⁵ Xavier Roy,⁵ Jean-Philippe Tetienne,^{1,*} and David A. Broadway^{1,†}

¹*School of Science, RMIT University, Melbourne, VIC 3001, Australia*

²*Institute of Materials Research and Engineering (IMRE), Agency for Science, Technology and Research (ASTAR), Singapore 138634, Singapore*

³*Department of Physics, University of Basel, Basel, Switzerland*

⁴*School of Physics, University of Melbourne, Melbourne, VIC 3010, Australia*

⁵*Department of Chemistry, Columbia University, New York, NY, USA*

⁶*Swiss Nanoscience Institute, University of Basel, Basel, Switzerland*

CONTENTS

S1. Experimental details	2
A. CrSBr thickness determination	2
B. Measurement sequence	2
S2. Analysis	3
A. Hysteric gap determination	3
S3. Micromagnetic simulations	4
S4. Additional data	4
A. Raman measurements	4
B. Other twisted monolayer transition	5
C. Other twisted bilayer transition	6
D. AFM switching transition in AFM-FM stack	7
References	9

* jean-philippe.tetienne@rmit.edu.au

† david.broadway@rmit.edu.au

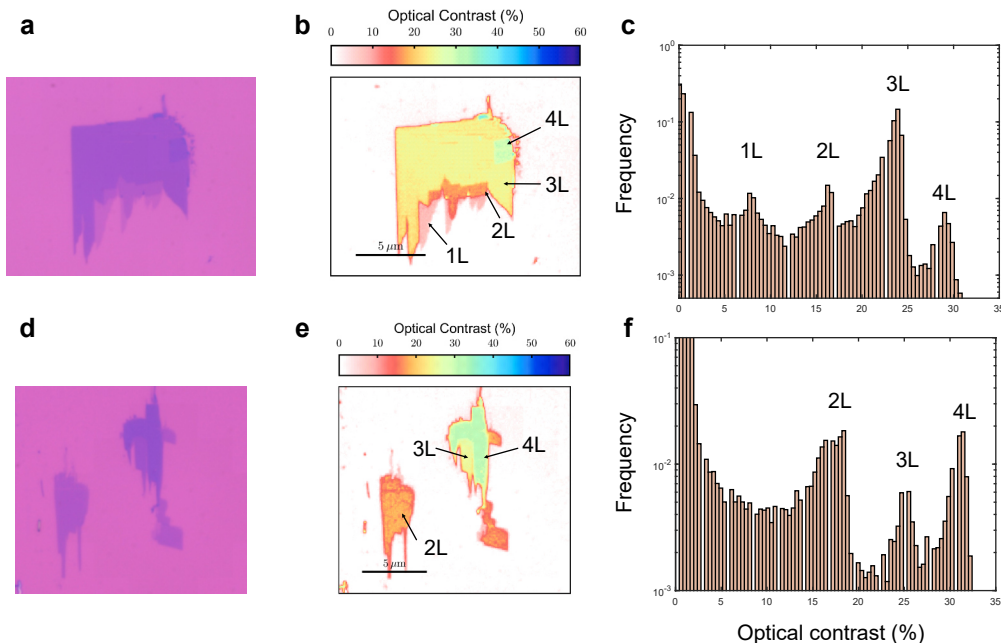


FIG. S1. Optical contrast of CrSBr flakes. **a** Optical image of a CrSBr flake exfoliated onto a SiO_2/Si substrate. **b** False colour contrast image processed from **a**. **c** Histogram of contrasts extracted from the image **b**. **d-f** As **a-c** for a different set of flakes. The 2L flake on the left hand side was used in the stack analysed in Fig. 3 of the main text.

S1. EXPERIMENTAL DETAILS

A. CrSBr thickness determination

In Fig. S1 we show how 1L, 2L, 3L, and 4L CrSBr flakes can be identified by their characteristic optical contrast of $\approx 7, 15, 24, 30\%$ respectively on the microscope used. We show two representative sets of flakes that feature a variety of thicknesses for illustration. This method was also validated by comparing the optical contrast to AFM data in Fig. S2.

B. Measurement sequence

Magnetic images were taken using continuous wave optically detected magnetic resonance (CW-ODMR). As depicted in Fig. S3(a), a single measurement sweep over n chosen MW frequencies takes place over $2n$ camera exposures, with every second being a “MW off” reference measurement. The laser is on throughout and the on/off MW cycle acts as an amplitude modulation to filter out drifts in (for example) laser power. The sequence is then repeated $N < 1000$ times (taking three hours or less) to acquire the desired SNR.

Although optimum sensitivity is in principle obtained by probing a single frequency, since widefield measurements probe a large field of view over which the NV ODMR line shape can vary with changing MW and laser power, capturing the full (or majority) of the resonance linewidth is incentivised to make the measurement robust against these inhomogeneities. Crystal strain within the diamond sensor, by changing the NV zero field splitting frequency, can also inhibit accurate magnetic mapping. Strain effects can be normalised out by taking a reference two-peak measurement, recording maps of the frequencies f_+ and f_- and taking the sum ($D = (f_+ + f_-)/2$). In our measurements the strain variation was negligible compared to the strength of the magnetic signals investigated.

Two schemes for acquiring sets of data were utilised in this work. Firstly, for Fig 1 of the main text, we used the sequence depicted in Fig. S3(b). In this case, a single low field measurement field $B_M \approx 5$ mT is held constant while a probe field B_p is varied between measurements. This scheme has the advantage of accessing any B_p within the range of the vector electromagnet (up to 1 T in any direction), including those that cannot be measured well using NV microscopy. This approach measures the remanent magnetisation and was appropriate for the FM-FM stack in allowing us to assess whether domains that form at higher fields are stable towards zero field.

For Figs. 2-4 of the main text we preferred the approach sketched in Fig. S3(c), where B_M also acts as the probe

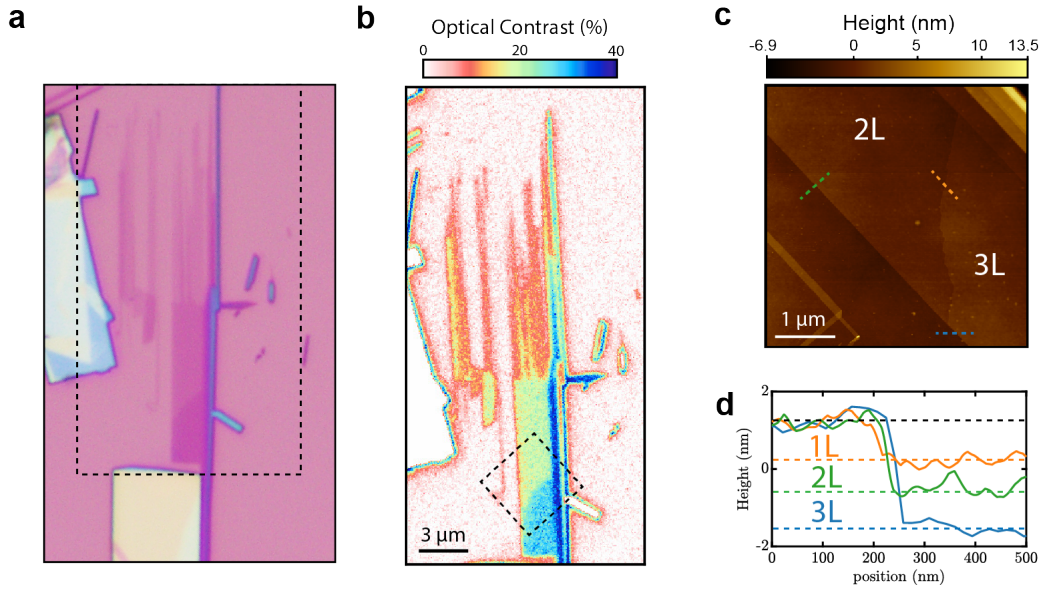


FIG. S2. Optical contrast comparison to atomic force microscopy. **a** Optical image of exfoliated CrSBr flake on SiO₂/Si substrate. **b** Optical contrast of the region highlighted in **a**. **c** Atomic force microscopy of the region indicated in **b**. **d** Line cuts of different atomic force microscopy steps as indicated in **c**.

field. This sequence is appropriate for stacks including AFM flakes which have fully compensated magnetisation at low fields and directly probing the magnetic behaviours across given transitions is important.

Prior to all measurement series, the NV axes (i.e. the $\langle 111 \rangle$ family of diamond axes) were determined by measuring the NV ODMR response at fields of ≈ 200 mT. This procedure is necessary to ensure optimal NV sensing since significant field misalignment will degrade measurement contrast. Since the symmetry axes of the CrSBr flakes were aligned within an estimated 3° of the true $\langle 110 \rangle$ diamond axes, the in-plane projections of the applied fields will not in general lie precisely along the targeted CrSBr b axis. However, given the strong magnetocrystalline anisotropy of CrSBr, this is only expected to make a minor difference to the results.

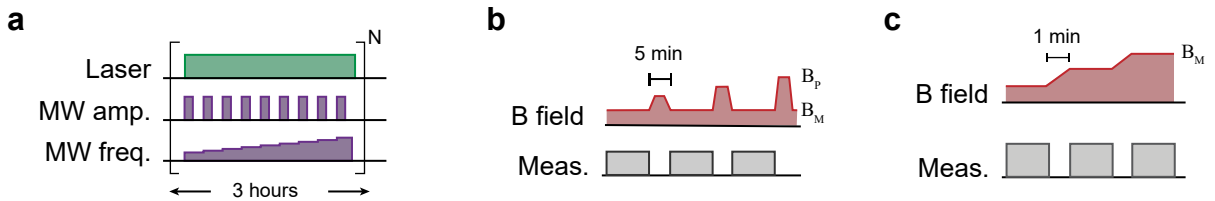


FIG. S3. Control sequences used. **a** NV-control and readout sequence where the NV spins are illuminated with a CW laser and the RF field has an amplitude modulation for normalisation and is swept over a range of frequencies. **b** Magnetic control sequence used for the 1L \times 1L sample shown in Fig.1 of the main text. The flake is initialised in a new magnetic state by pulsing the magnetic field up to a value B_p and then reduced to a near zero magnetic field for NV measurements. **c** Magnetic control sequence used in all other samples, where the measurement and setting fields were identical.

S2. ANALYSIS

A. Hysteric gap determination

To obtain a more reliable estimation of the central magnetic field and the hysteresis gap, we take the difference in the sweep directions and fit this transition with a Lorentzian function. The twisted region has a smaller width $\Delta_T = 32(17)$ mT ($\Delta_B = 51(25)$ mT) and is centred at a slightly lower magnetic field $B'_T = 191(4)$ mT ($B'_B = 195(5)$ mT).

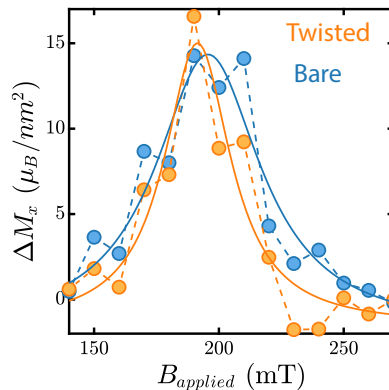


FIG. S4. Difference in the magnetic hysteresis for the twisted (orange) and bare (blue) sections of the bilayer flipping with a twisted FM interaction shown in Figure 2 of the main text and Lorentzian fits (solid lines).

S3. MICROMAGNETIC SIMULATIONS

To gain qualitative insight into the importance of various parameters on the behaviours observed, we carried out micromagnetic simulations of some of the scenarios investigated in the main text. The simulations are based directly on the model developed in Ref.,^{S1} and we use the same set of parameters unless stated differently. In brief, black and white images of each layer that are deduced from optical images of the flake are used to define the geometry. The layered structure of CrSBr is then mimicked at hand of the finite difference mesh by setting the cell thickness to the thickness of one CrSBr layer. Exchange coupling between layers is set to a negative, small fraction of the inplane exchange coupling, facilitating a-type anti-ferromagnetic ordering. Small AFM or FM defects within a stack are used as nucleation points for the respective domains.

To simulate the 1L(FM)-2L(AFM) stack the finite element mesh is set to a size of 1200 x 600 x 3 cells with corresponding cell sizes of 4 nm x 4 nm x 0.8 nm, respectively. This is significantly scaled down to obtain reasonable computation times. The exchange coupling between the two flakes is set to the same value ($-0.008 \cdot A_{ex}$, with A_{ex} : inplane exchange stiffness) as the interlayer coupling within a flake. No strain related spatial variation of the intralayer exchange coupling is used in these simulations. Results of this simulation are shown in Fig. S11, and discussed in the corresponding section.

The 2L(AFM)-2L(AFM) stack is simulated with a mesh size of 1200 x 1000 x 4 cells and corresponding cell sizes of 4 nm x 4 nm x 0.8 nm, respectively. Fig. S5 shows simulations for the bilayer flipping transition (Fig. 3 main text). We estimate the strain profile across the stack from the Raman measurements, and adjust the interlayer exchange coupling accordingly. We compare the behaviour in dependence of the applied field in the twisted and bare regions, both with and without exchange coupling across the twisted interface (for simplicity we take the pristine interlayer exchange coupling). This allows to assess whether the intraflake exchange interaction could be responsible for the observed low field forced-FM behaviour. The hysteresis loop is repeated ten times in order to generate some statistics. A few of these runs were taken out due to malfunctions in the simulation.

The onset of the flipping transition is indeed earlier than in the bare region in the simulations, but this behaviour does not appear to be linked to the inclusion of the exchange term. In fact, the hysteresis is narrower when the interflake exchange is added. These simulations indicate that interflake exchange plays a minor role in this case and structural defects likely dominate.

S4. ADDITIONAL DATA

A. Raman measurements

The Raman map shown in Fig. 3 was collected on a Horbia LabRAM Raman spectrometer using a 1800 lines/mm grating, a 532 nm Ventus laser and a 100 \times (NA=0.8) air objective resulting in a spot size of approximately 2 μ m in diameter. The laser power was kept to 2.8 mW (as measured before the objective) to avoid laser heating or damage of the sample. In Fig. S6 we present more detailed analysis of this data. A typical CrSBr Raman spectrum is shown in Fig. S6(a), showing the P2 and P3 Raman lines. Both lines are modulated by strain and are observed to vary across the stack, as summarised by the histograms of fit peak locations Fig. S6(b), where a Lorentzian lineshape was used

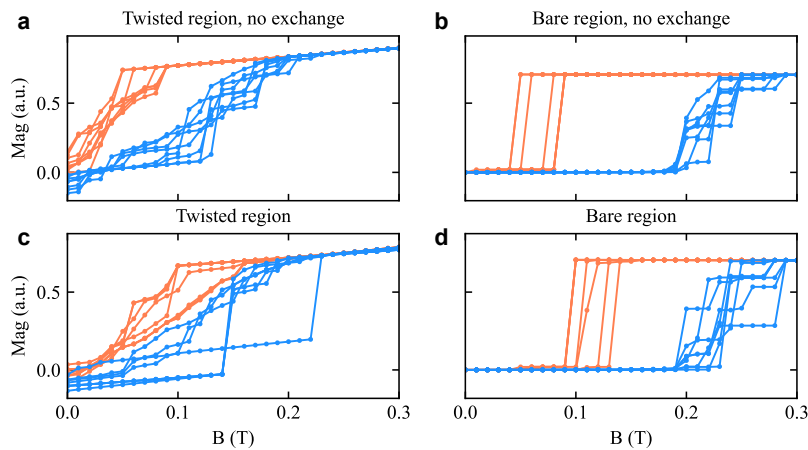


FIG. S5. Micromagnetic simulations of the 2L-2L stack (Fig. 3 in the main text). The average magnetisation within the twisted (left; **a**, **c**) and bare twisted (right; **b**, **d**) regions for multiple simulations both without (top; **a**, **b**) and with (bottom; **c**, **d**) interlayer exchange coupling between the flakes. Sweeping increasing the applied field in the positive direction are coloured in blue while decreasing sweeps are coloured in orange.

for the fit. Maps of the peak locations, intensity, and width are shown in Fig S6(c) for P2 and Fig. S6(d) for P3. The features are broadly similar, however for the main text we focussed on the P3 line since it is less sensitive to the number of layers present in a stack.

The increased width in peaks fit within the top flake (the transition of which we analysed in Fig. 3 of the main text) highlights that there could be significant strain variation below the diffraction limit of the Raman measurement.

To confirm that there was no significant strain from large structural defects from the stacking process (for example bubbles), we took atomic force microscope images of the entire stack on the diamond sensor after all of the other measurements (Fig. S7). While the roughness of the diamond and it’s metallic capping layer prohibit high resolution topography, we still do not observe any large changes that could explain the strain observed in this stack. This suggests that the strain could be due to lattice mismatch of the twisted stacks.

B. Other twisted monolayer transition

In Fig. S8(a) we show the switching transition of the monolayer not shown in the main text. The transition has step-like features but is generally smoother than that shown in the main text, occurs at lower fields (< 60 mT), and over a wider span of field strengths (about 40 mT). The magnetisation reconstruction for this set of data is generally more prone to artefacts due to the aligned flake’s small size compared to both the measurement spatial resolution and the thicker sections of the orthogonal flake. To circumvent the issue, for this set of reconstructions we confine M_y magnetisation to the target monolayer while allowing M_x to be placed anywhere within the stack. We note that even with this procedure, the reconstructed magnetisation is lower than for a typical saturated monolayer, which is an artefact incurred by NV magnetometry when the magnetic domain size approaches the measurement spatial resolution. We can see in Fig S8(b), where select normalised magnetic images at extreme points in the transition are presented, that domains again appear to nucleate in (and are initially confined to) the twisted region. However, due to the extremely small size of any “bare” regions or regions that overlap with thicker twisted flakes, we do not include traces of their evolution in Fig. S8(a). Instead, we show M_x (triangular points) averaged over the same regions as in the main text, showing that the magnetisation in the other flake appears unchanged across this transition.

The broad and reproducible switching transition observed in this case allows us to consider a final experiment, wherein we initialise one flake (“primed”) into a multi-domain state using a field of ≈ 35 mT and sweep across the switching transition of the orthogonal flake (“unprimed”). This experiment allows us to further test the hypothesis that domain walls in one flake can influence (or be influenced by) magnetisation in the other due to the local spin (anti)alignment.

In this case (data summarised in Fig. S9(a)) we see a sharp transition in the twisted region of the unprimed flake (given by the M_x magnetisation), which is accompanied by the M_y magnetisation from the primed flake saturating as we can see in the images Fig S9(b). Compared to the data shown in Fig. 1 of the main text, the FM switching transition onset in this case is later (80 mT versus 67.5 mT). While the difference may simply be due to the stochastic nature of domain nucleation, it may also hint at a relative increase in energy cost for domain nucleation in the

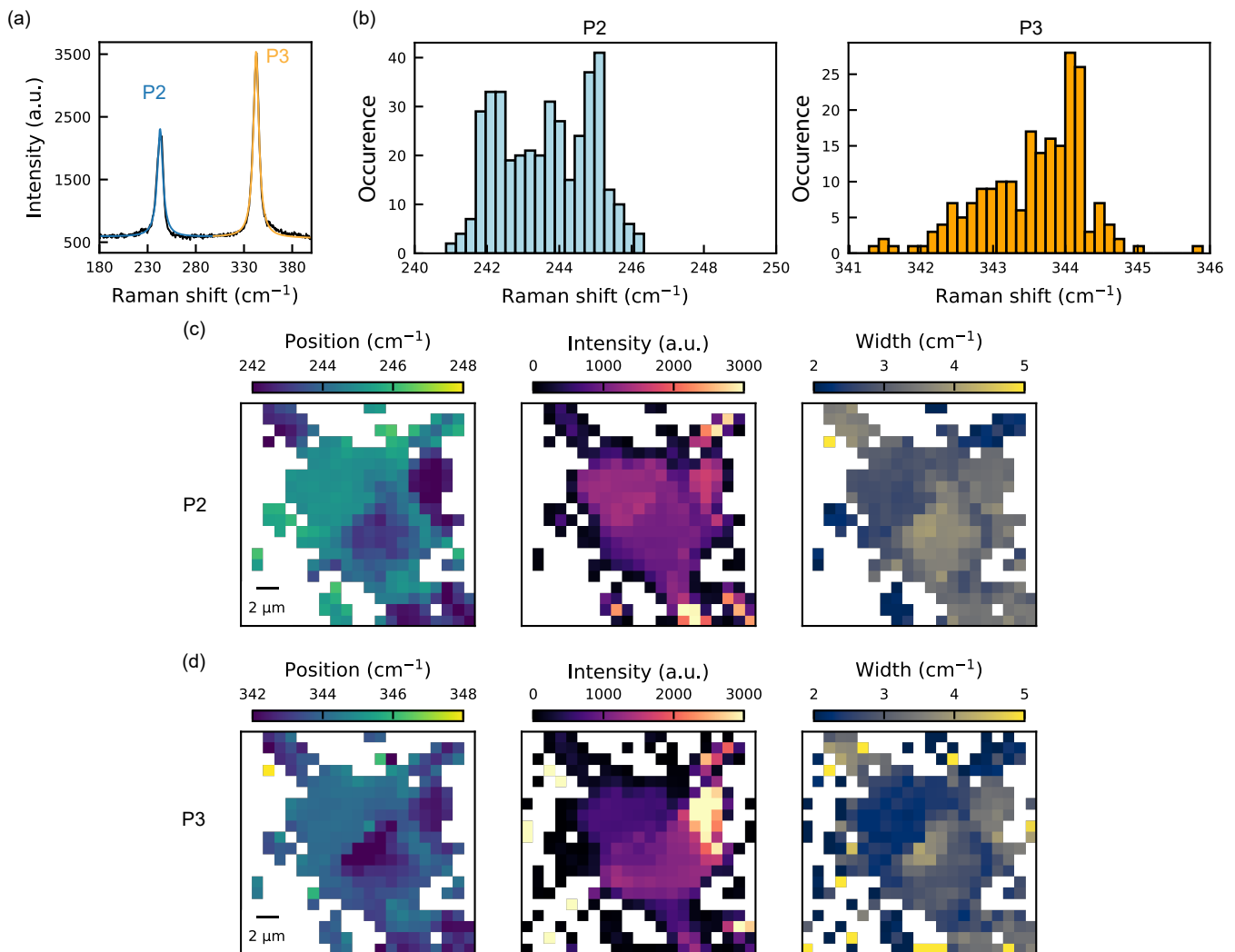


FIG. S6. Spatial Raman measurements of the AFM-AFM stack. **a** Exemplary Raman spectrum from a single pixel. **b** Distribution of the shift of the P2 (left panel) and P3 (right panel) Raman lines for the AFM-AFM stack. **c** Lorentzian fits results for the position, intensity, and width of the P2 Raman line on the AFM-AFM stack, where an intensity threshold was used to remove areas containing no CrSBr. **d** Same as in **c** but for the P3 Raman line.

unprimed flake due to the scrambled state of the primed flake. We also do not observe the domain border alignment with the a (b') axis within the twisted region that we saw in Fig. 1. The small flake sizes relative to our measurement spatial resolution and the potential impact of conflating variables such as stacking-induced strain do not allow us to make definitive conclusions in this case, however these results, combined with those shown in Fig. 4, are suggestive of a non-trivial magnetic interaction across the twisted interface.

C. Other twisted bilayer transition

In Fig. S10(a) we show the hysteresis observed when sweeping the applied magnetic field along the y axis. In this case, we do not observe strong magnetic signals at low field or an offset hysteresis as for the other bilayer phase transition. Instead, a narrower hysteresis loop is observed in the twisted region, similar to the results in Fig. 2 of the main text. The difference between the two behaviours within the same twisted stack hints at factors other than exchange interactions across the twisted interface being important in determining the magnetic properties. Namely, as the top flake in this stack was observed to be more highly strained (c.f. Fig. 3(b)), it is likely that the extra level of strain plays a role in enabling some of these behaviours.

Along with the narrower hysteresis, we again observe that the strength of the magnetisation in the twisted region

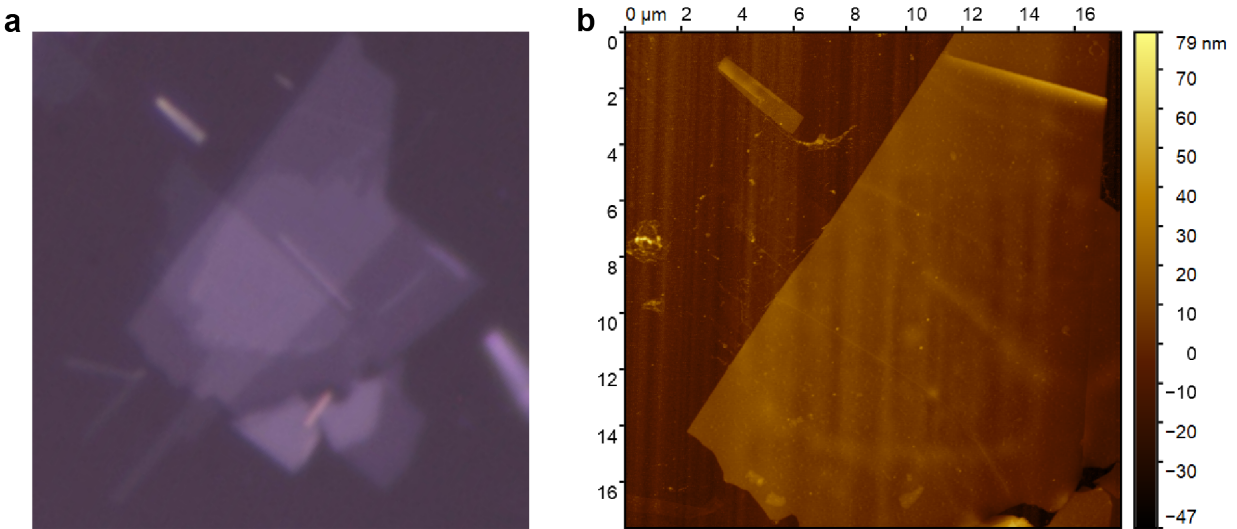


FIG. S7. Atomic force microscopy of the AFM-AFM stack. **a** Optical image of the AFM-AFM stack of the PDMS stamp during transfer **b** Topography of the stack on the diamond taken with an atomic force microscope.

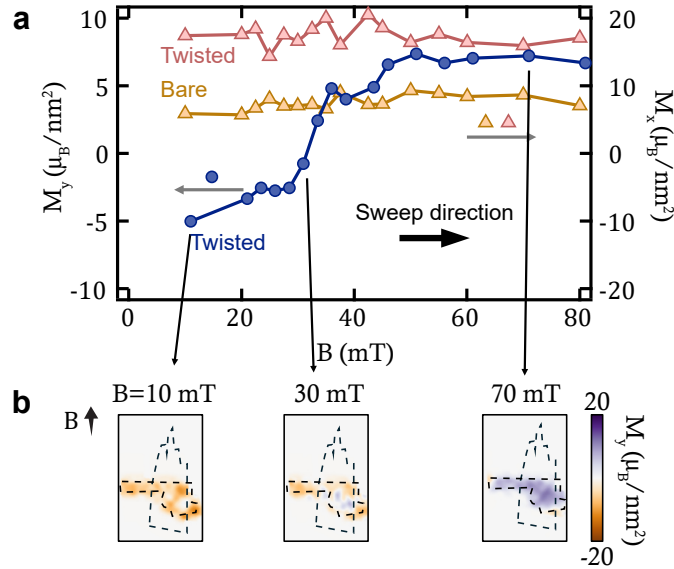


FIG. S8. (a) Monolayer flipping data for the flake not shown in Fig. 1 of the main text. M_y shows the transition and we also plot M_x to show that it is unchanged both in the twisted region and in the bare (orthogonal) monolayer across this transition. (b) Images showing the switching transition, showing domain nucleation in the twisted region.

is stronger after the phase flip than in the bare region. The increase in magnetisation is sudden and only present during the forced FM state, meaning it is not easily explained by a gradual canting of the misaligned flake.

D. AFM switching transition in AFM-FM stack

In Fig. 2 of the main text we saw that the AFM switching transition in an AFM-FM stack onset earlier in the twisted region, and exhibit a narrower hysteresis loop. In Fig. S11 we present results from micromagnetic simulations of this stack, modelled as a bilayer-monolayer system for computational simplicity. Figure S11(a) shows the total simulated magnetisation in the twisted region (the same as shown in Fig. 2(e) in the main text), with the projection M_x seen to closely resemble the data from Fig. 2(d). Notably, the net magnetisation is nonzero before the bilayer flipping transition and is above the value for a saturated bilayer afterwards. Figure S11(b) and (c) show the contributions

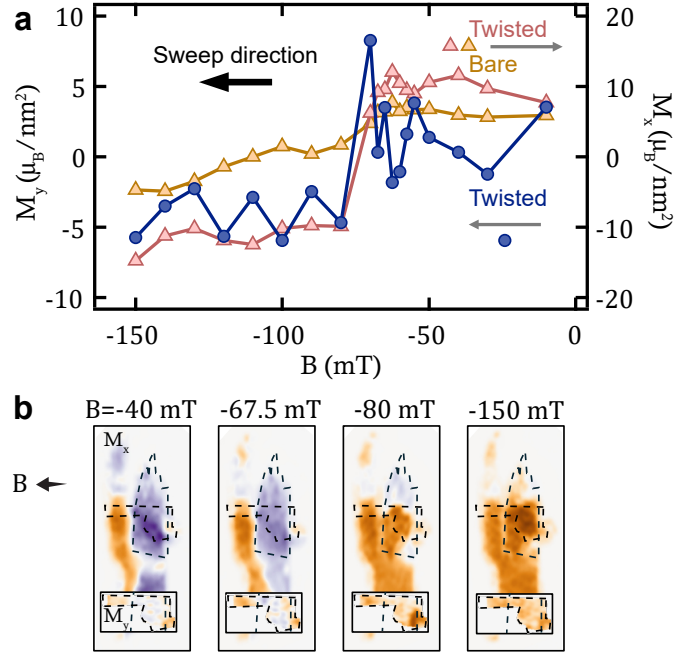


FIG. S9. (a) Summary of the FM switching transition sweeping along the y direction with the orthogonal (primed) flake initialised in a partially-switched state. (b) Select images from the series in (a), showing M_x with M_y inset in all cases.

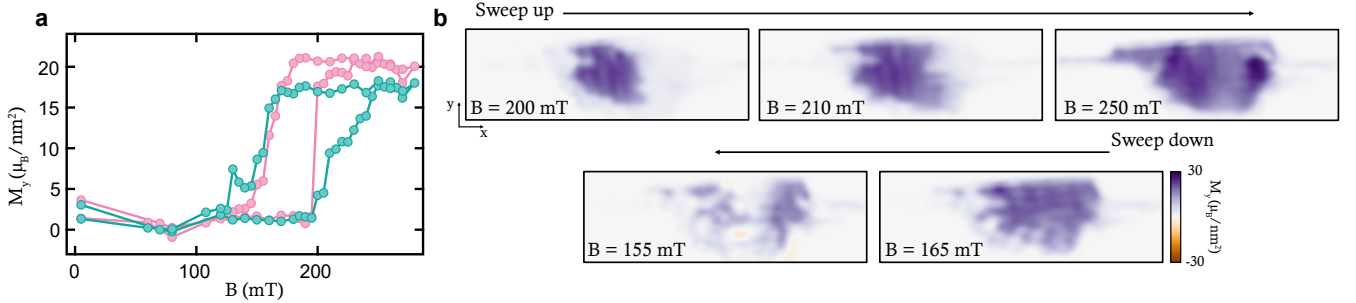


FIG. S10. (a) Hysteresis loop for the bilayer transition observed when sweeping fields along the y direction. Twisted region shown in pink, bare region in cyan. (b) Exemplary images from the measurement series in (a).

just from the bilayer and monolayer, respectively. Here we can see that the FM layer cants steadily towards the x axis with increasing field and, if nonzero exchange is assumed, acts to inhibit the full flipping of the bilayer. When the bilayer flips fully, the corresponding increase in M_x is almost totally offset [c.f. Fig. S11(a)] by a reduction in monolayer M_x . Upon decreasing the field after saturation, we see that the monolayer hysteresis matches the width of that of the bilayer transition.

Since the contributions from individual layers cannot be measured in our experiment, we are unable to directly confirm the simulated picture. However, we can turn to the reconstructed M_y component from the experimental dataset as we can see from Fig. S11(c) that any hysteresis in monolayer spin reorientation is evident in both magnetisation projections. In Fig. S12(a) we plot the average reconstructed M_y magnetisation in the twisted region, normalised against the bare bilayer (the same data shown in Fig. 2(d) inset). A positive magnetisation from the FM layer is always observed, however an increase is observed across the AFM switching transition (example images shown in Fig. S12(b)). Unlike in the simulations, the observed M_y hysteresis is narrower than (and slightly offset from) the bilayer transition. Nevertheless, these results do appear to suggest that the FM layer reorients across the bilayer flipping transition. As in the simulations, a nonzero exchange interaction across the twisted interface is a candidate cause, although it is also difficult to rule out confounding factors such as strain.

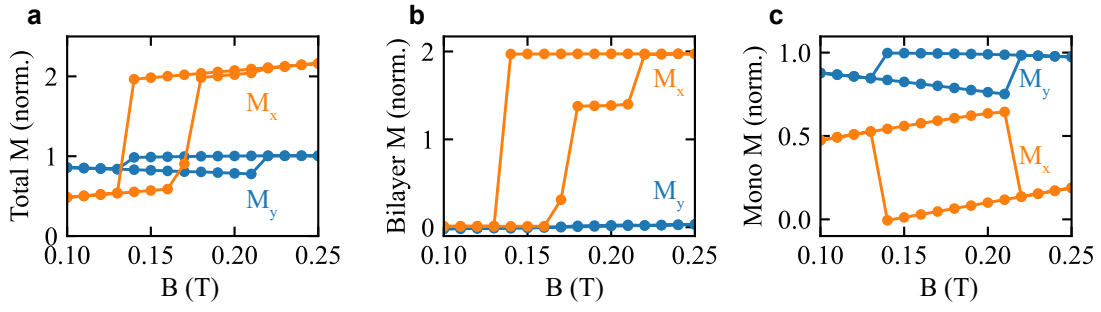


FIG. S11. (a) Results of a micromagnetic simulation of the experiment from Fig. 2 of the main text. The net magnetisation in the twisted region (modelled as a 2L-1L system for computational simplicity) is calculated and decomposed into M_x (orange) and M_y (blue) components. The magnitude is normalised against the magnetisation corresponding to a saturated CrSBr monolayer. (b) As (a) but only for the bilayer. (c) as (a) but only for the FM layer.

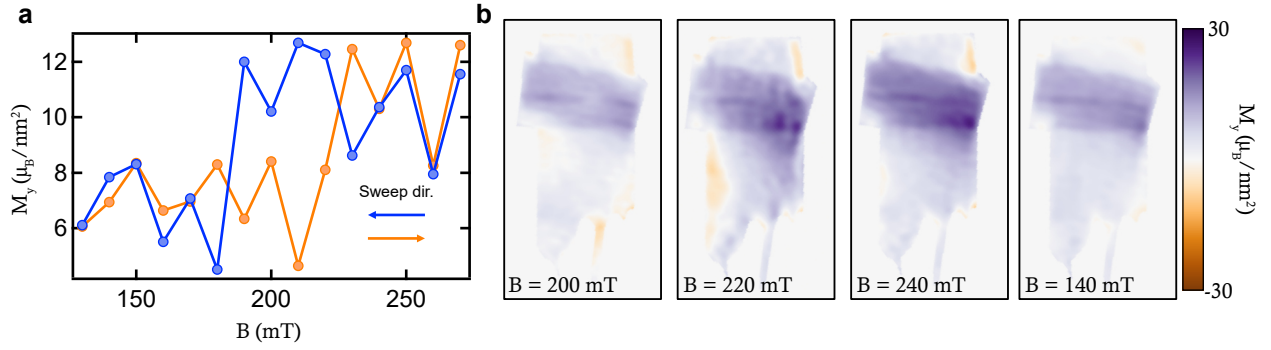


FIG. S12. (a) M_y hysteresis loop observed for the data from the sweep shown in Fig. 2 of the main text. The values plotted are averages from within the twisted region, with the average from the bare region subtracted. (b) Selected M_y images from this series.

[S1] Tschudin, M. A. *et al.* Imaging nanomagnetism and magnetic phase transitions in atomically thin CrSBr. *Nature Communications* **15**, 6005 (2024)